Physicochemical Aspects of the Movement of the Rieske Iron Sulfur Protein during Quinol Oxidation by the bc_1 Complex from Mitochondria and Photosynthetic Bacteria†

Antony R. Crofts,*,‡ Sangjin Hong,‡ Zhaolei Zhang,§ and Edward A. Berry*,§

Center for Biophysics and Computational Biology, University of Illinois at Urbana−Champaign, Urbana, Illinois 61801, and Lawrence Berkeley National Laboratory, University of California, Berkeley, California 94720

Received April 27, 1999; Revised Manuscript Received August 16, 1999

ABSTRACT: Crystallographic structures for the mitochondrial ubihydroquinone:cytochrome *c* oxidoreductase (bc_1 complex) from different sources, and with different inhibitors in cocrystals, have revealed that the extrinsic domain of the iron sulfur subunit is not fixed [Zhang, Z., Huang, L., Shulmeister, V. M., Chi, Y.-I., Kim, K. K., Hung, L.-W., Crofts, A. R., Berry, E. A., and Kim, S.-H. (1998) *Nature (London), 392*, 677−684], but moves between reaction domains on cytochrome c_1 and cytochrome *b* subunits. We have suggested that the movement is necessary for quinol oxidation at the Q_o site of the complex. In this paper, we show that the electron-transfer reactions of the high-potential chain of the complex, including oxidation of the iron sulfur protein by cytochrome c_1 and the reactions by which oxidizing equivalents become available at the Q_o site, are rapid compared to the rate-determining step. Activation energies of partial reactions that contribute to movement of the iron sulfur protein have been measured and shown to be lower than the high activation barrier associated with quinol oxidation. We conclude that the movement is not the source of the activation barrier. We estimate the occupancies of different positions for the iron sulfur protein from the crystallographic electron densities and discuss the parameters determining the binding of the iron sulfur protein in different configurations. The low activation barrier is consistent with a movement between these locations through a constrained diffusion. Apart from ligation in enzyme−substrate or inhibitor complexes, the binding forces in the native structure are likely to be $\leq RT$, suggesting that the mobile head can explore the reaction interfaces through stochastic processes within the time scale indicated by kinetic measurements.

Structures for the ubiquinol:cytochrome *c* oxidoreductase (bc_1 complex)[1] from several mitochondrial sources have recently been solved crystallographically (*1*−*5*). Xia et al. (*1*) identified the location of the [2Fe-2S] center in their crystals of the beef heart mitochondrial complex, but the protein was disordered, and they were unable to assign structure. The center was further from cyt c_1 than expected from the rapid electron transfer reactions observed experimentally (*6*−*10*). They discussed several possible mechanism for redox exchange over this distance, including electron transfer through the protein, a substantial conformational change between oxidized and reduced forms of the ISP, and the possibility that the disorder might arise from a mobility of the subunit that could be functionally important. In our native structures from chicken, rabbit, and two different crystal forms of the beef complex, the ISP was relatively well ordered, and the extrinsic domain (the mobile head) was close to cyt c_1. However, the distances from the [2Fe-2S] center to the heme Fe differed by as much as 4 Å between different structures (*2*), being closest in hexagonal $P6_522$ crystals of the beef mitochondrial complex, where the His-161 was within H-bonding distance of the heme c_1 propionate. We suggested that this was the likely configuration for electron transfer, and Iwata et al. (*3*) have reached the same conclusion from similar $P6_522$ crystals. After

† We acknowledge with gratitude the support for this research provided by NIH Grants GM 35438 (to A.R.C.) and DK 44842 (to E.A.B.) and by the Office of Health and Environmental Research, U.S. Department of Energy, under Contract DE-AC03-76SF00098 (E.A.B.).

* Corresponding authors: for functional aspects, A.R.C., Center for Biophysics and Computational Biology, University of Illinois at Urbana−Champaign, 388 Morrill Hall, 505 S. Goodwin, Urbana, IL 61801; for structural aspects, E.A.B., Structural Biology Division, Lawrence Berkeley National Laboratory, 250 Melvyn Calvin Lab 5230, University of California, Berkeley, CA 94720-5230.

‡ University of Illinois.

§ University of California.

[1] Abbreviations: bc_1 complex, ubihydroquinone:cytochrome *c* (or c_2) oxidoreductase; b_H, higher potential cytochrome *b* heme; b_L, lower potential cytochrome *b* heme; *p*-BQ, *p*-benzoquinone; cyt, cytochrome; DAD, 2,3,5,6-tetramethyl-*p*-phenylenediamine; DQ, duroquinone; EDTA, ethylenediaminetetraacetic acid; $g_x = 1.80$ signal, electron paramagnetic resonance spectral band at this *g* value associated with the presence of quinone and reduced iron sulfur protein together in the bc_1 complex; ISP, iron sulfur protein; ISP^{ox} and ISP^{red}, oxidized and reduced states of the iron sulfur protein; ISP_B or ISP_C, the iron sulfur protein docked at cytochrome *b* or cytochrome c_1 interfaces, respectively; 2-OH-1,4-NQ, 2-hydroxy-1,4-naphthoquinone; MOA, β-methoxyacrylate, or similar group, the pharmacophore of a class of inhibitors acting at the Q_o site; NQ, naphthoquinone; P^+ and P, oxidized and reduced forms of the primary donor of the photochemical reaction center; PES, *N*-ethylphenazonium ethosulfate; PMS, *N*-methylphenazonium methosulfate; QH_2, ubihydroquinone or quinol; Q, ubiquinone or quinone; Q_i site, quinone reducing site; Q_o site, quinol oxidizing site; RC, photochemical reaction center; SQ, semiquinone; UHDBT, 5-*n*-undecyl-6-hydroxy-4,7-dioxobenzothiazol; UHNQ, 3-undecyl-2-hydroxy-1,4-naphthoquinone.

10.1021/bi990963e CCC: $18.00
Published on Web 11/05/1999

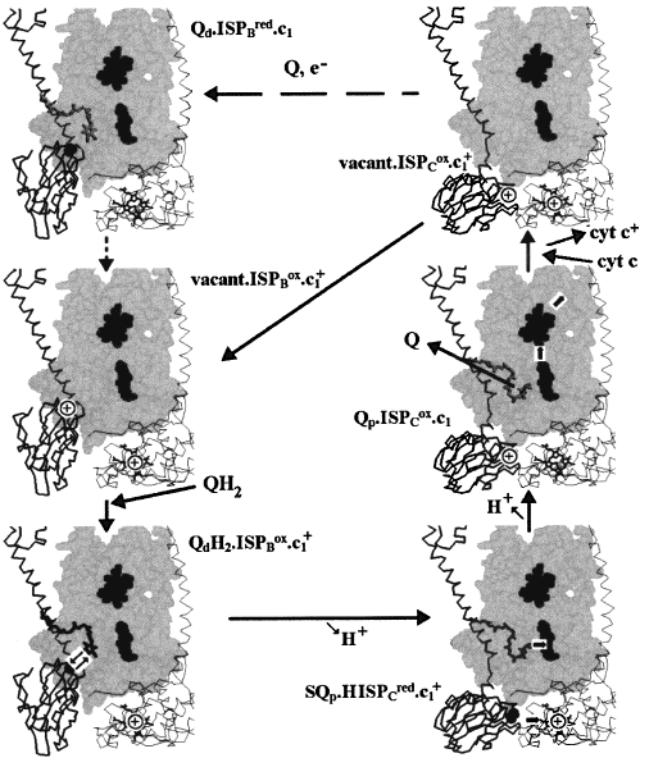

FIGURE 1: Scheme showing the reactions of involved in quinol oxidation. The complex is shown in six different states. The state vacant·ISP_Box·c_1^+ is the complex with a vacant Q_o site and ISP_B oxidized; upon binding quinol the reaction complex, Q_dH_2·ISP_Box·c_1^+, is formed, with quinol in the distal domain of the Q_o site, and oxidized ISP docked on cyt *b*; SQ_p·$HISP_C^{red}$·c_1^+ is the intermediate formed after the transition state, in which H-transfer has occurred, the semiquinone has flipped to the proximal domain, and the reduced ISP has moved to cyt c_1; Q_p·ISP_C^{ox}·c_1 is the product-bound complex; vacant·ISP_C^{ox}·c_1^+ is the complex after dissociation of quinone and oxidation by cyt c^+. The state Q_d·ISP_B^{red}·c_1 represents the complex between quinone and reduced ISP_B that forms the $g_x = 1.80$ signal, which is not in the reaction cycle.

cocrystallization with stigmatellin, a Q_o site inhibitor known to interact strongly with the reduced form of the ISP (ISP^{red}) (*11*), the ISP was found in a different position, close to the Q_o site (*2*). The conserved liganding domain (head) had moved by a rotational displacement from a site in contact with cyt c_1 in the native structure to a concave interface on cyt *b* close to the binding pocket containing the inhibitor. This position brought the [2Fe-2S] center close to that found in the native structures from the work of Xia et al. (*1*). Connections between the ISP and the inhibitor in our electron density maps have been modeled as H-bonds between Nϵ of His-161 and carbonyl and methoxy O-atoms of the stigmatellin ring (*2*). From the distance between reaction partners, and the constraints on rates of reaction, none of the structures so far available would be competent in all partial reactions necessary for quinol oxidation. We have therefore suggested that the movement of the ISP mobile domain between interfaces on cyt c_1 and cyt *b* is a necessary part of the catalytic mechanism, as summarized in Figure 1 (*2*, *5*, *12*, *13*). An additional position for the ISP mobile domain has been demonstrated by Iwata et al. (*3*) in a new crystal form of the bovine complex, $P6_5$. One monomer had the ISP in a new position, intermediate between those found in previous structures (*1*, *2*), and the other had a disordered ISP. Kim et al. (*4*) have recently located the ISP structure in the crystals of Xia et al. (*1*) and also noted displacements of the [2Fe-2S] cluster induced by inhibitor binding.

We have discussed in companion papers (*13*, *25*) aspects of the structure and the movement of the ISP head that relate to mechanism. Several groups have discussed mechanisms in which a "catalytic switch" controls delivery of reducing equivalents to the ISP^{ox} and suggested that the movement of the ISP is controlled by protein binding changes linked to redox events outside the immediate reactions of quinol oxidation (*3*, *4*). In this paper we report measurements of the kinetics of electron transfer through the bc_1 complex in chromatophores from the photosynthetic bacterium *Rhodobacter sphaeroides*. The mitochondrial complexes have evolved from those in ancestors from the α-proteobacteria (*14*), and the catalytic subunits have been well conserved across the bacterial−mitochondrial divide. The bacterial complexes have a simpler subunit complement (*15*, *16*), but the complex performs the same function as in the mitochondrial chain, oxidizing ubiquinol through a modified Q-cycle mechanism (*6*, *17*−*21*). However, the kinetics can be more readily measured in situ on a rapid time scale because the electron-transfer chain can be populated with stoichiometric amounts of substrates (QH_2 as reductant and ferricyt c_2 as oxidant) by flash illumination to activate the photochemical reaction center. The partial reactions contributing to reactions at each of the catalytic sited of the bc_1 complex can be separately measured through use of redox poising and specific inhibition of one or the other site. We show here that the reactions that involve movement of the ISP are rapid compared to the rate-limiting step. We measure the activation energies of these processes and conclude that they do not determine the overall activation barrier measured for quinol oxidation. The occupancies of the ISP in different configurations of the complex have been estimated from the crystallographic electron densities of the extrinsic domain in native crystals and in cocrystals with stigmatellin, UHDBT, myxothiazole, or MOA-type inhibitors. We discuss values for the binding constants determining occupancy, calculated from the electron densities in different states. We conclude that, except for the ligation involved in formation of enzyme−substrate complexes or with the Q_o site occupant, the forces constraining the ISP to the positions observed in native crystals are relatively weak. We discuss the mobility of the complex in the light of these binding forces and a stochastic model in which the mobile head of the ISP explores the reaction domain through a simple constrained diffusion.

MATERIALS AND METHODS

Estimation of Occupancies at Different ISP Positions. The CCP4 program ICOEFL was used to determine what linear combination of the sets of calculated structure factors best fits the observed amplitudes for the native and inhibitor containing crystals (*22*−*25*). For any defined set of electron densities, the program calculates a scale factor and a *B*-factor, where the scale factor is proportional to occupancy and the *B*-factor is derived from the temperature factor, which is a measure of the disorder at each atom. Negative *B*-factors indicate that the density is better ordered in the partial structure than in the overall model. For calculation of occupancy, the data from residues 71−196 (the mobile head) and the [2Fe-2S] cluster were used. The ISP membrane anchor was included in the "non-ISP" portion.

Table 1

	ISP_C head	app. K_A^{ISPc}	ISP_B head	app. K_A^{ISPB}	unaccounted
native chc	0.494	1.20	0.095	0.23	0.411
native chb	0.573	1.34	0.0003	0.001	0.426
native chm	0.558	1.41	0.048	0.12	0.394
MOA-inh	0.529	1.12	−0.003	0.0	0.471
myxothiazole	0.540	1.17	−0.005	0.0	0.460
stigmatellin	0.000		0.925	12.32	0.075
UHDBT	0.368	1.10	0.265	0.72	0.367
extra Q	0.655	1.96	0.010	0.03	0.335

Table 2

ISP distal 1		ISP proximal 1		
occupancy	K_A	occupancy	K_A	unaccounted 1
0.464	1.10	0.118	0.28	0.419
ISP distal 2		**ISP proximal 2**		
occupancy	K_A	occupancy	K_A	unaccounted 2
0.519	1.27	0.074	0.18	0.407

Table 3

	monomer 1				
	ISP^1_C	K_A	ISP^1_B	K_A	unacc
native	0.54	1.29	0.04	0.10	0.42
stigmatellin	0.11	1.1	0.82	11.7	0.07
Stg + antimycin	0.01	0.1	0.89	8.9	0.10
UHDBT	0.34	0.94	0.30	0.83	0.36
MOA-inhibitor	0.67	2.09	0.01	0.03	0.32
	monomer 2				
	ISP^2_C	K_A	ISP^2_B	K_A	unacc
native	0.70	2.69	0.04	0.15	0.26
stigmatellin	0.11		1.03	>100	0.0
Stg + antimycin	0.06		0.99	>100	0.0
UHDBT	0.49	2.33	0.30	1.43	0.21
MOA-inhibitor	0.91	11.4	0.01	0.125	0.08

For Table 1, the calculated occupancies were obtained from the raw data by dividing the global scale factor observed in the ISP protein by that in the non-ISP protein and assuming a full occupancy for the non-ISP part. This gave the fractional occupancies of the ISP head in the different positions. Since the total ISP must sum to 1.0 (as indicated by the data with stigmatellin), we could also assign a value to the unaccounted occupancy. This was obtained by summing the occupancies at both positions of the mobile head and subtracting that value from 1.0. If we assume this unaccounted density represents unbound ISP head, we may equate it with ISP_{free} to provide a quantitative measure of the relative binding affinities of different states, shown as apparent association constants, K_A, for the ISP in the ISP_C or ISP_B position, as indicated by the superscript.

For Table 2, the mobile domain of ISP_C, in the configuration distal from cyt *b*, was fit independently on the two monomers of the native crystals. The ISP_B, in the configuration proximal to cyt *b*, was fit in two separate calculations, since the program ICOEFL only allows manipulation of four sets of data. The ISP head in the alternative monomer was set to zero.

For Table 3, a least-squares refinement of position and occupancy was performed separately for five different structures (native and four different inhibitor combinations), and the structural parameters were assigned to five different groups of atoms: (1) protein other than ISP but including the anchoring span of ISP (residues 1−70) (non-ISP) (2) ISP^1_B, the ISP mobile head (residues 71−196) in the proximal (to heme b_L) position in monomer 1; (3) ISP^1_C, the ISP mobile head in the position close to cyt c_1 in monomer 1; (4) ISP^2_B, the ISP mobile head in the proximal position in monomer 2; and (5) ISP^2_C, the ISP mobile head in the position close to cyt c_1 in monomer 2. Non-ISP was fixed at unit occupancy.

Measurement of Cytochrome Kinetics. Kinetic traces were obtained essentially as previously described (*6*), with specific conditions as detailed in the figure captions. All experiments were performed in an anaerobic cuvette, with the redox potential monitored, and changed by addition of small aliquots of dithionite or ferricyanide to reduce or oxidize the suspension. Redox mediators, inhibitors, etc., when present are described in the figure legends. For experiments determining the activation energy, traces were recorded at different temperatures, as monitored by a thermometer in the cuvette. Rate constants were estimated from the kinetic traces by fitting the curves using exponential functions (one component for cyt *b* reduction, two components for cyt *c* oxidation), assuming pseudo-first-order kinetics, using the graphics program Origin 5.0 (Microcal Software, Inc., Northampton, MA). For cyt *b* reduction, relative rate constants were also measured by recording the maximal rate after the lag phase. The relative rate constant for quinol oxidation was determined from the rate of cyt b_H reduction (*6*, *18*, *19*). The redox potential was adjusted so that the initial concentration of quinol in the membrane was the same before each experiment, and flash excitation generated oxidant in the same relative stoichiometry. The initial concentration of reactants was therefore the same, and the rate therefore directly reflected the rate constant. For cyt *b* kinetics, only the portion of the curve after the lag phase was used.

The activation energies found in this work differ somewhat from those previously reported. We attribute the difference primarily to a better measurement of the temperature of the reaction medium in the present experiments. In the earlier work, a thermistor was placed outside the cuvette and between it and the water jacket. Although the thermostated cuvette housing was enclosed by insulation, the stirring was from above, leaving an uninsulated surface. In the present experiments, the stirring was from below, and the temperature was monitored directly by a thermometer in the medium.

RESULTS AND DISCUSSION

Modified Q Cycle, and Role of the High-Potential Chain in Oxidation of Quinol. The reactions involved in oxidation of quinol have been discussed at length in companion papers (*13*, *25*). The reactions are catalyzed by three subunits: cyt *b*, containing two *b*-type hemes, b_L (lower potential heme) and b_H (higher potential heme); cyt c_1, containing heme c_1; and the iron sulfur protein, containing a [2Fe-2S] center. Quinol is oxidized at the Q_o site of the complex. Quinol oxidation occurs in a bifurcated reaction, in which one electron is transferred to a high-potential chain and the other to a low-potential chain. The high-potential chain, consisting of the ISP, cyt c_1, and cyt *c* (or c_2), transfers the first electron

from quinol to an acceptor (cytochrome oxidase in mitochondria, the oxidized photochemical reaction center in photosynthetic systems), leaving a semiquinone at the Q_o site. The semiquinone is undetectable during normal turnover, so the reaction at the Q_o site appears to be a concerted electron transfer to the high- and low-potential chains. The low-potential chain consists of the two cyt *b* hemes, which serve as a pathway through which electrons are transferred across the coupling membrane from the Q_o site to the Q_i site, at which quinone is reduced to quinol. To provide the two electrons at the Q_i site required for reduction of quinone, the Q_o site oxidizes 2 equiv of quinol in successive turnovers. The first electron at the Q_i site generates a relatively stable semiquinone, which is reduced to quinol by the second electron.

Kinetics in the High-Potential Chain in the Presence of Myxothiazole or UHDBT. In *Rb. sphaeroides*, oxidizing equivalents from the primary donor (P^+/P) of photochemical reaction center (RC) are delivered to cyt c_1 by cyt c_2, with a $t_{1/2}$ of about 100−200 μs, depending on temperature and cyt c_2 content of the chromatophores (*5*, *13*, *20*). The electron-transfer from the Rieske center to cyt c_1 cannot be resolved, because it is not rate-determining. A minimal value for the rate constant has been determined from the kinetics of cyt *c* turnover, taking advantage of the fact that inhibitors of class I (stigmatellin, UHDBT, or UHNQ), prevent the [2Fe-2S] center from reducing cyt c_1 (by binding preferentially to the reduced form and raising the $E_{m,7}$ value; *11*, *26*−*28*), but inhibitors of class II (myxothiazole and MOA-type inhibitors) do not (*27*−*29*). Both classes of inhibitor prevent quinol oxidation by binding at the site normally occupied by the quinol (*1*−*4*, *11*, *26*−*33*). In the presence of either class, since quinol is prevented from binding and delivering electrons to the reactants, the electron transfer chain is simplified so that only the high-potential chain is available for photooxidation. Because excitation with a sufficiently short and intense flash activates all reaction centers, but only once, electrons and holes are introduced into the chain in stoichiometric amounts. In chromatophores from wild-type cells under normal growth conditions, the ratio of RC:cyt c_2:bc_1 complex is close to 2:1:1 (*18*, *19*), so that a flash provides enough holes to oxidize ~2 one-electron carriers in each chain:

$$2P^+ + 2\ \text{ferrocyt}\ c_2 = 2P + 2\ \text{ferricyt}\ c_2^+\ (\sim 1\ \mu s) \quad (1a)$$

$$[\text{2Fe-2S}]\cdot\text{ferrocyt}\ c_1 + \text{ferricyt}\ c_2^+ = [\text{2Fe-2S}]\cdot\text{ferricyt}\ c_1^+ + \text{ferrocyt}\ c_2\ (\sim 150\ \mu s) \quad (1b)$$

$$[\text{2Fe-2S}]\cdot\text{ferricyt}\ c_1^+ = [\text{2Fe-2S}]^+\cdot\text{ferrocyt}\ c_1 \quad (\ll 150\ \mu s) \quad (1c)$$

$$[\text{2Fe-2S}]^+\cdot\text{ferrocyt}\ c_1 + \text{ferricyt}\ c_2^+ = [\text{2Fe-2S}]^+\cdot\text{ferricyt}\ c_1^+ + \text{ferrocyt}\ c_2 \quad (1d)$$

Overall, in the presence of myxothiazole:

$$2P^+ + [\text{2Fe-2S}]\cdot\text{ferrocyt}\ c_1 = 2P + [\text{2Fe-2S}]^+\cdot\text{ferricyt}\ c_1^+ \quad (1)$$

With UHDBT or stigmatellin present, and the properties of the [2Fe-2S] center modified (shown by [2Fe-2S]*):

$$2P^+ + \text{ferrocyt}\ c_2 + [\text{2Fe-2S}]^*\cdot\text{ferrocyt}\ c_1 = 2P + \text{ferricyt}\ c_2^+ + [\text{2Fe-2S}]^*\cdot\text{ferricyt}\ c_1^+ \quad (2)$$

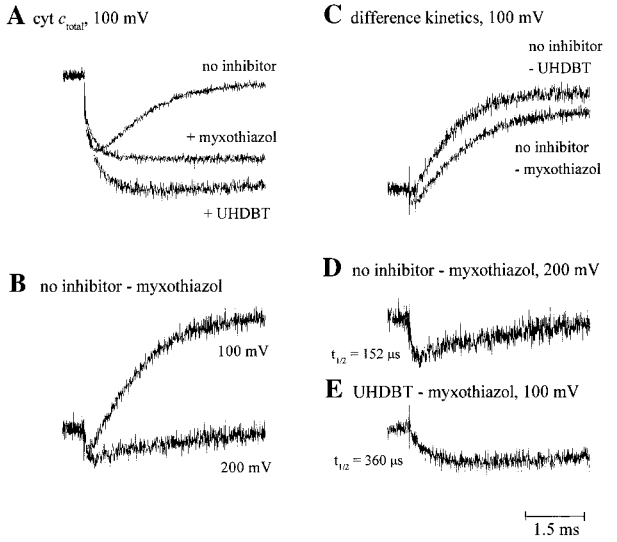

FIGURE 2: Kinetics of the high-potential chain measured through absorbance changes of the *c*-type cytochromes. Kinetic changes were measured in the absence of inhibitor and in the presence of myxothiazole (5 μM) or UHDBT (10 μM). Chromatophores of *Rb. sphaeroides* Ga were suspended in 100 mM KCl and 50 mM MOPS (pH 7.0) to a concentration of 0.5 μM reaction center with the following redox mediators: 1 μM each 2-OH-1,4-NQ and pyocyanin; 2 μM each DAD, PES, and PMS; 10 μM each *p*-BQ, 1,2-NQ, 1,4-NQ, and DQ. Also present were 2 μM each valinomycin and nigericin and 1 mM ferric sodium EDTA. Traces shown were the average taken from 20, with 180 s between measurements, and are the difference between kinetics measured at 551 and 542 nm (*13*). The instrument response time was <10 μs, and the ambient redox potential (E_h) was adjusted to 100 or 200 mV by addition of small aliquots of dithionite or ferricyanide. (A) Traces at 100 mV; (B) difference between traces taken without and with myxothiazole, at E_h 100 or 200 mV; (C) difference between traces taken without and with either UHDBT (top curve) or myxothiazole (bottom), at E_h 100 mV; (D) difference trace from panel B at E_h 200 mV, at larger scale, with the fast phase fitted by a first-order decay; (E) difference between traces with UHDBT and with myxothiazole, at larger scale, with the fast phase fitted by a first-order decay.

The electrons will come from the components with lowest E_m value. In the presence of myxothiazole, the electrons come from cyt c_1 and the [2Fe-2S] center, which then remain oxidized on the 100 ms time scale. The cyt c_2, although it is initially rapidly oxidized by P^+, becomes rereduced as the lower E_m components are oxidized (reaction 1 above) (*6*, *7*). In the presence of UHDBT (or stigmatellin or UHNQ), no electrons are available from the [2Fe-2S] center, so the flash-induced change is an oxidation of cyt c_1 and cyt c_2 only (reaction 2) to give an absorbance change of larger amplitude when measured at 551−542 nm, at which both *c* cytochromes absorb with a similar extinction coefficient (*6*, *7*, *11*, *33*; and see Figure 2). The extra amplitude of the flash-induced cyt *c* change after addition of UHDBT is due to the inhibition of electron transfer from the [2Fe-2S] center (*11*, *33*). This contribution can be assayed from the difference between the kinetics with myxothiazole present and those with UHDBT present (Figure 2). In the traces shown, the chromatophore preparation had less cyt c_2 than in "standard"

preparations (RC:c_2:bc_1 of 2:0.8:1, instead of 2:1:1), so the $t_{1/2}$ for oxidation of cyt c_1 was a little greater (170 μs at 30 °C), some cyt c_2 remained oxidized in the presence of myxothiazole, and the increased amplitude induced by UHDBT was less than we have previously reported (*6*, *7*, *33*, *29*).

If the electron donation from [2Fe-2S] to cyt c_1 were slow compared to the oxidation of cyt c_1, one would expect that the *c*-type cytochrome oxidation kinetics would first rise to the level seen with UHDBT present and then decay to the myxothiazole level, with a rate reflecting the transfer of electrons from the reduced [2Fe-2S] center. No trace of any such a transient is observed in the changes measured in the presence of myxothiazole alone (*6*, *29*). We have interpreted this as indicating that the rate of electron transfer from the [2Fe-2S] center to cyt c_1 is rapid compared to the rate of oxidation. Because the E_m value for the ISP is higher than that for cyt c_1 (*7*, *11*), the rate of reduction by ISP^{red} must match the rate of oxidation by cyt c_2 when the reactants for the former process are far from favorable, requiring that the rate constant is greater by a factor of at least 10. In a kinetic model of these reactions, Crofts and Wang found that a rate constant for oxidation of the [2Fe-2S] center in the range $>10^5$ s^{-1} provided a good fit (*6*). Tsai et al. (*8*) concluded that the rate was also rapid in mitochondrial complexes. The activation energy for these reactions in *Rb. sphaeroides*, assayed from the kinetics in the presence of myxothiazole, and the difference kinetics with UHDBT, was much lower than for quinol oxidation (*5*).

Contribution of the ISP Movement to the Kinetics of the High-Potential Chain. In the work of Crofts and Wang (*6*) and in the earlier work of Meinhardt and Crofts (*29*), it was observed that the kinetics of cyt *c* oxidation ± myxothiazole in the 100 μs range differed, so that the rise kinetics appeared to be slower in the presence of the inhibitor. This effect was then unexplained, but the new structural results have prompted us to reexamine this phenomenon. The contribution of the ISP to the kinetics of the high-potential chain could be observed from the differences in kinetics in the presence and absence of myxothiazole or UHDBT (Figure 2). At E_h ~ 200 mV in the absence of inhibitor, since the quinone pool is oxidized before the flash, the Q_o site cannot turn over until a quinol arrives from the reaction center, with a delay of ~1 ms (*18*). The kinetics of the cyt *c* changes in the first millisecond therefore reflect only the activity of the high-potential chain. The changes (cyt c_{total}) were measured at 551−542 nm, where both cyt c_1 and cyt c_2 contribute equally. The fast phase ($t_{1/2}$ < 10 μs) was due to cyt c_2 oxidation, and the slower oxidation phase reflects cyt c_1 oxidation. However, the amplitude at ~3 ms reflects the oxidation of only ~1 equiv of cyt *c*, since the oxidation of cyt c_1 occurs at the expense of cyt c_2, and their extinction coefficients are nearly the same at this wavelength pair. In these experiments, the difference kinetics ± myxothiazole in the ~200 μs range showed a small overshoot (see Figure 2). The crystallographic evidence suggests that, in the presence of myxothiazole, most of the ISP is in the ISP_C configuration (see below for data and discussion of the association constant), from which reaction occurs in the ≤10 μs time scale. In the absence of myxothiazole, some fraction of the ISP will likely be in the ISP_B position, since the ISP is reduced and the quinone pool is oxidized, and these are the conditions in which the ISP interacts with quinone to give a changed EPR spectrum, with a band at g_x = 1.800 (*30*−*32*). In terms of the states shown in Figure 1, the most straightforward interpretation of the overshoot is therefore that, in a fraction of complexes, the arrival of the electron on cyt c_1 from the ISP is delayed because of the association of the ISP in formation of this complex. Since the complex requires ligation of quinone in the Q_o site with ISP^{red} in the ISP_B position, the delayed electron transfer would reflect the dissociation of this complex and movement from ISP_B to ISP_C positions. The amplitude of the overshoot was about 20% of the change attributable to cyt c_1. However, this amplitude could be explained either by a model in which the overshoot represents a small fraction of centers in this configuration, with a relatively slow reaction time, or a model in which a large fraction is initially in ISP_B, and has a relatively rapid reaction time. If all complexes had the ISP bound in the ISP_B configuration, then the reaction time indicated by the small overshoot would suggest a process with a half-time in the range ~30 μs. Alternatively, the kinetics may indicate that ~20% of complexes are in the ISP_B configuration and that the complex between Q and ISP^{red} is relatively long-lived ($t_{1/2}$ ~3 ms). The rise kinetics of the overshoot obviously cannot be faster than the rate of oxidation of cyt c_1 and do not measure directly the kinetics of oxidation of the ISP.

When similar experiments were performed at E_h ~ 100 mV (quinone pool ~30% reduced, Q_o site >80% occupied by QH_2), the kinetics showed a rereduction of cyt *c* as electrons were delivered to the high-potential chain from the Q_o site. Under these conditions, the overshoot was still observed but was more transient and reversed in ~200 μs (Figure 2). The fraction of centers in which quinone would be complexed with ISP_B^{red} at E_h 100 mV compared to E_h 200 mV could be estimated from the apparent E_m of the g_x = 1.800 signal (~90 mV, similar to that of the pool). From this value, 0.7 of the centers with the g_x = 1.800 signal at E_h 200 mV would have the signal at 100 mV. Centers with the g_x = 1.800 signal would have ISP initially in the ISP_B position, and the mobile head would have to have moved to the ISP_C position in order to transfer an electron to cyt c_1 during the 200 μs transient.

It should be noted that the complex between quinol and ISP_B^{red} is not an intermediate of the normal catalytic cycle, and the relatively long decay time of the overshoot seen when the pool is initially oxidized does not have a significance in normal turnover.

Kinetics of Quinol Oxidation. In addition to the measurements of cyt *c* kinetics above, the kinetics of turnover of the Q_o site also provide constraints on the reactions and displacements of the ISP. The oxidation of quinol can be followed in chromatophores from *Rb. sphaeroides* by observing the rate of reduction of cyt b_H following flash illumination (*6*, *7*, *34*; and see Figure 3). Since the reactions in the *b*-heme chain are much more rapid than the delivery of electrons to the chain from the Q_o site (*6*, *34*), the electron transfer from the Q_o site can be assayed when electrons are prevented from passing from cyt b_H to the Q_i site by antimycin. The kinetics show a second-order dependence on quinol concentration, and the rate saturates as the pool becomes reduced. Maximal rates ($t_{1/2}$ ~1 ms at 20 °C, pH 7) are seen with the pool partially oxidized, suggesting a

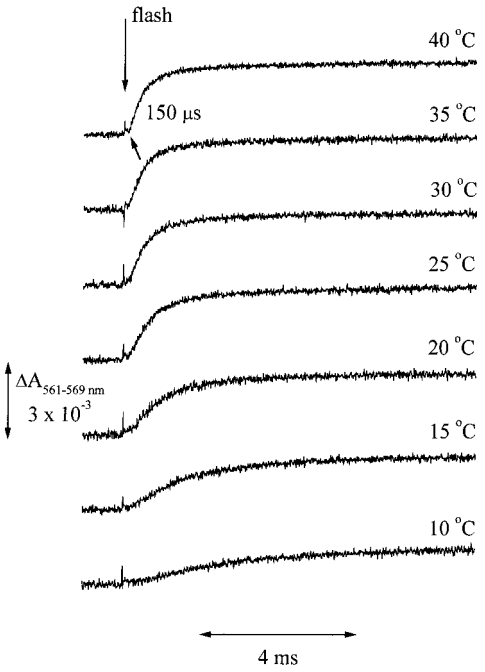

FIGURE 3: Kinetics of quinol oxidation, measured through the reduction of cyt b_H in the presence of antimycin, and variation in rate with temperature. Chromatophores of *Rb. sphaeroides* Ga were suspended in 100 mM KCl and 50 mM MOPS (pH 7.0) containing 10 μM of antimycin to a concentration of 0.5 μM reaction center with the following redox mediators; 1 μM each 2-OH-1,4-NQ and pyocyanin; 2 μM each DAD, PES, and PMS; 10 μM each *p*-BQ, 1,2-NQ, 1,4-NQ, and DQ. Also present were 2 μM each valinomycin and nigericin and 1 mM ferri-sodium EDTA. Traces shown were the average taken from 20, with 60 s between measurements, and show the difference kinetics between 561 and 569 nm (*13*). The instrument response time was <10 μs. The redox potential was 115 mV at 10 °C and then shifted downward 5 mV for every increase of 5 °C, as suggested in ref *5*. The vertical arrow indicates the flash activation.

tighter binding of QH_2 than Q. Under these experimental conditions (E_h ~100 mV), the reactions at the Q_o site are delayed by a short lag (~150 μs). This lag reflects the time taken for an oxidizing equivalent produced in the photochemical reactions to reach the site through turnover of the high-potential chain and therefore contains information about the processes of the high-potential chain, including the movement from the ISP_C to the ISP_B position (see below for further discussion). For the reverse displacement, the transient overshoot in cyt *c* oxidation discussed above limits the time to <200 μs when the pool is partly reduced (see above). These values are maximal times for the entire electron-transfer process, including binding and unbinding, diffusion, and electron transfer. Times for these processes can also be estimated from a consideration of the turnover of the complex in the absence of inhibitor. Under uninhibited conditions, 2 equiv of QH_2 are oxidized at the site following a single-turnover flash (*18*), and the overall process can be followed through the electrogenic reactions associated with electron transfer between Q_o and Q_i sites through the low-potential chain (*18*, *35*). These can readily be measured through the slow phase of the electrochromic carotenoid absorbance change ($t_{1/2}$ ~ 2 ms). The electrogenic reactions follow a continuous monotonic kinetics, without any indication of a kinetic break, suggesting that all processes contributing to the second turnover, including the displacements of the ISP in the high-potential chain to regenerate an oxidant at the Q_o site, and replacement of Q by QH_2, are much faster than the rate-determining step.

Activation Barriers in Quinol Oxidation. Crofts and Wang (*6*) explored the temperature dependence of the reactions leading to quinol oxidation in chromatophores from *Rb. sphaeroides*. They showed that the oxidation of quinol had the same value for activation energy for different states of the quinone pool. With the pool 30% reduced, the kinetics were assayed at pH 7 through reduction of cyt b_H, while at pH 8.9, the kinetics were measured by reduction of cyt b_L. Both reactions showed a similar maximal rate and activation energy. Under conditions in which the pool was initially oxidized, turnover of the Q_o site (assayed through cyt b_H reduction) was slower and occurred with a ~1 ms lag, attributed to delivery of QH_2 from the reaction center, as discussed above. However, the activation barrier was the same as when the pool was partly reduced. Because the local concentration of quinol did not affect the activation energy, Crofts and Wang (*6*) concluded that the reactions associated with binding of quinol could be excluded as the source of the activation barrier. Crofts and Wang (*6*) also measured the reactions of the high-potential chain in the presence of myxothiazole or UHDBT and showed that the oxidation of cyt c_{total} in the presence of either inhibitor and the difference kinetics with UHDBT and myxothiazole (arising from the availability of an electron on the ISP in the presence of myxothiazole) all had relatively small activation barriers. They therefore excluded these processes as the location of the larger activation barrier seen in the cyt b_H reduction kinetics.

In light of the new structural information, we have reinvestigated the activation barriers of the partial reactions of quinol oxidation in order to see if the movement of the ISP from cyt c_1 to cyt *b* contributes to the activation barrier, as has been recently suggested (*36*). Kinetic traces showing the temperature dependence of oxidation of cyt c_{total} in the presence or absence of myxothiazole, and the "overshoot" revealed in the difference kinetics, are shown in Figure 4. The oxidation rates, with or without inhibitor, increased over the range from 10 to 40 °C, with an activation energy of ~25 kJ mol^{-1}, but were substantially faster over this entire range than cyt b_H reduction.

The overshoot was little affected by temperature change. If the movement of the ISP had a higher activation barrier than the reactions leading to oxidation of cyt c_1, the overshoot would have *increased* in amplitude on lowering the temperature, rather than the small loss of amplitude observed at lower temperatures. The results show that the contributing processes had either lower activation barriers or kinetics much faster than the rate-determining step (the ~150 μs oxidation of cyt c_1).

Although no direct information about the activation energy of these more rapid processes can be obtained from these traces, it is clear that oxidation of the ISP and its movement are more rapid than the rate-limiting step at all temperatures and will not contribute to the activation barrier for quinol oxidation.

In addition to the direct measurements from cyt *c* kinetics, the kinetic lag before onset of reduction of reduction of cyt b_H (to monitor quinol oxidation; *6*, *18*) provides hitherto unnoted information about the reactions delivering oxidizing equivalents to the Q_o site. These include the movement from

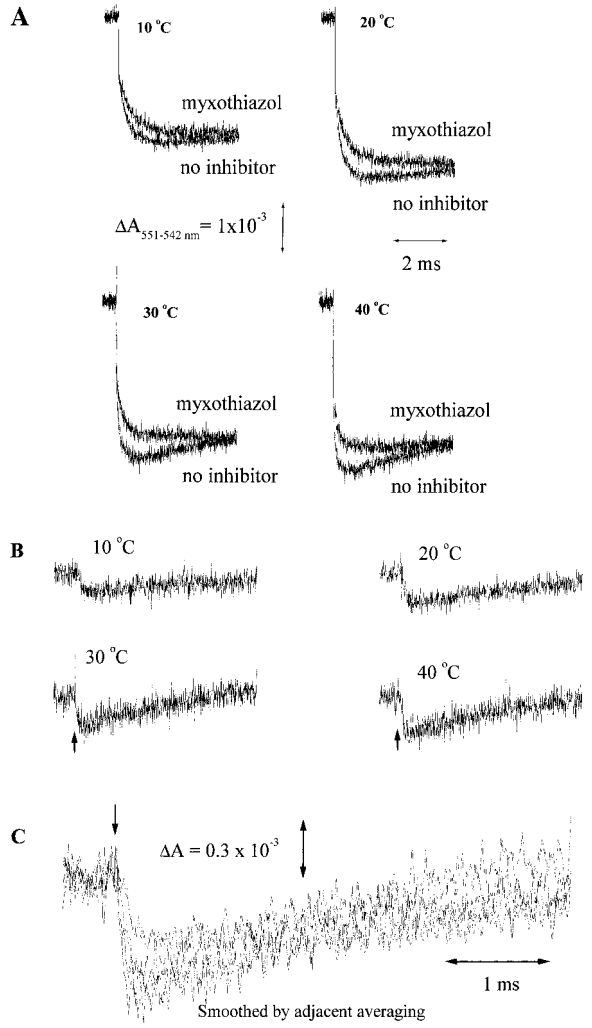

FIGURE 4: Temperature dependence of reactions in the high-potential chain. The reactions were measured through variation in the rate of cytochrome *c* oxidation with temperature. Conditions were as for Figure 2, but ambient potential was maintained at 200 mV. Kinetic curves after the flash were deconvoluted into two first-order components. One of these in the ~10 μs range accounted for ~50% of the change and was attributed to cyt c_2 oxidation. The second phase in the 100−300 μs range was used to provide the rate constants shown in Figure 5, assuming pseudo-first-order kinetics and constant starting concentrations of reactants over the temperature range investigated. (A) Kinetics of cyt c_{total} oxidation following flash illumination in the absence or presence of myxothiazole (upper traces) at E_h ~200 mV. (B) Difference kinetics, showing the kinetics of the overshoot at different temperatures. (C) Comparison of overshoot kinetics on a larger scale. The curves were smoothed by adjacent averaging.

ISP_C to ISP_B positions. We have therefore repeated these experiments at higher time resolution to measure the temperature dependence and activation energy for the lag (Figure 5).

The temperature dependence of cyt b_H reduction, measured with the quinone pool ~30% reduced, is shown in Figure 3. The strong temperature dependence over the range 10−40 °C is obvious from inspection. In the experiment shown, the activation energy derived by fitting the best straight line to the points was 47 kJ mol^{-1}, but this was biased by the stronger temperature dependence at lower temperatures, and values in similar experiments varied between 40 and 56 kJ mol^{-1}. The value from the slope between 15 and 40 °C for cyt b_H reduction was ~37 kJ mol^{-1}, closer to that previously

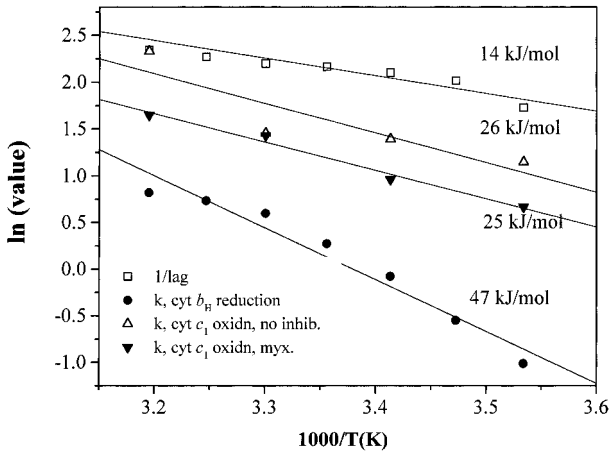

FIGURE 5: Arrhenius plots of data from Figures 3 and 4. Rate constants were estimated from the kinetic traces by fitting the curves with exponential functions, as indicated in the legends to Figures 3 and 4, assuming pseudo-first-order kinetics. The values for rate constants are in units of reciprocal milliseconds. The lag before cyt b_H reduction was measured (in milliseconds) by extrapolating the best straight-line fit to the initial linear portion of the reductive phase, to the baseline level before the flash. The value plotted is ln (1/lag), to give units comparable to those for ln *k*. Symbols are as indicated in the figure.

reported (*6*). The nonlinearity of the Arrhenius plot is discussed further below. In contrast to the temperature dependence of the rate of cyt *b* reduction, the traces show that the lag before onset of reduction was not strongly temperature-dependent. The lag was 180 ± 50 μs at 15 °C and 130 ± 50 μs at 40 °C, and the activation energy was ~14 kJ mol^{-1}. Much of the lag can be attributed to the time taken for oxidizing equivalents to arrive at [2Fe-2S] ($t_{1/2}$ ~150 μs for oxidation of cyt c_1). Since the E_m value for cyt c_1 (~270 mV) is a little lower than that for the [2Fe-2S] center (~290−300 mV at pH 7), oxidation of the latter lags a little behind that of the former. This constrains estimation of the contribution of movement to the lag and suggests that diffusion from the ISP_C to the ISP_B position must occur in <100 μs. Since neither the lag nor the overshoot in cyt c_1 oxidation shows an activation energy comparable to that for cyt *b* reduction, it seems unlikely that the movement of the ISP contributes to the activation barrier for quinol oxidation. This result is therefore in contradiction to the observation of Tian et al. (*36*), who noted an inhibited rate and increased activation energy for strains with mutations in the linker region of the ISP, when electron transfer was assayed by a steady-state approach. The authors did not indicate how they identified the contribution to the partial reactions involving the ISP, or if they had eliminated other possible contributions of the mutation to the properties of the ISP. Mutations that lower the E_m value of the cluster also show an inhibited rate (*37*−*39*) and an increased activation energy (*38*), but this is attributable to the direct contribution to the $\Delta G°'$ for formation of the semiquinone (*6*, *38*).

The Arrhenius plot for cyt *b* reduction was not linear and showed a much steeper slope at lower temperatures, suggesting that the reaction is not simple. At 10 °C, the kinetics were slower than expected from the slope obtained at higher temperatures. The lower slope to the Arrhenius plot at higher temperatures may in part be due to the fact that the reactions of the high-potential chain, because they have a lower

activation energy, contributed increasingly to limitation of the kinetics as the temperature was raised (*6*).

In summary, the kinetic evidence suggests that none of the reactions involved in delivery of oxidizing equivalents to the Q_o site is rate-limiting in quinol oxidation and none has a high enough activation energy to account for the value seen in cyt *b* reduction.

Role of Distance in Determining the Rate of Electron Transfer from the [2Fe-2S] Center to cyt c_1. The positions of the ISP in different structures, and the distance between the [2Fe-2S] center and reaction partners, have been discussed at length elsewhere (*2*, *13*, *25*; PDB files 1bcc, 2bcc, and 3bcc). Three positions of the [2Fe-2S] center are of importance in the present discussion: the stigmatellin-induced position in the chicken complex [which is close to that in the beef complex of Xia et al. (*1*), as calculated from the data they provided], the position in the native chicken complex, and the position in the native beef hexagonal complex, which shows the closest approach to cyt c_1.

The structural context of electron transfer theory has been much studied recently, and a consensus has emerged on the parameters of importance in determining rate constants. Three factors are of critical importance: distance, the standard free-energy change for the reaction, and the coupling, or reorganization energy, λ, from Marcus theory (see ref *40* for review). An important point on the energy v. reaction coordinate surface is the condition under which the products parabola intersects the reactant parabola at its minimum (when E_{act} is zero). Under these conditions $\lambda = -\Delta G°$ and the reaction proceeds at its maximal rate, with rate constant ($k°_{ET}$) normalized to this condition. Values for $k°_{ET}$ can be found experimentally by measuring the rate constant for a reaction under conditions giving different values for $\Delta G°$. Moser et al. (*9*) have measured reactions in photochemical reaction centers and adjusted values so as to span the range about the $\Delta G°$ giving this maximal value for $k°_{ET}$. From these results, and an extensive literature on other reactions, they have produced an empirical equation (Dutton's ruler) relating rate to distance:

$$\log k°_{ET} = 15 - 0.6R - 3.1(\Delta G° + \lambda)^2/\lambda$$

Here R is the edge-to-edge distance in angstrom units, and $\Delta G°$ and λ are expressed in electron volts. Similar work from Gray and Winkler (*10*) has led to some refinement of this picture in terms of secondary structure but with similar values for critical terms defining the ruler.

Applying this formula to the distance between centers in the structure of Xia et al. (*1*) under the condition when $\lambda = -\Delta G°$, we obtain a maximal rate constant of 2.5×10^{-4} s^{-1} for the 31 Å center-to-center distance and 2.5×10^{-1} s^{-1} when a 4 Å adjustment is made for the edge-to-edge distance. The corresponding distances in the native structure of Zhang et al. (*2*), from the chicken heart complex give rate constants of 166 s^{-1} and 1.66×10^5 s^{-1}, respectively, and the other complexes solved by Zhang et al. (*2*), which have shorter distances, have correspondingly more rapid rate constants. Clearly, the only distances that would permit electron transfer on the time scale measured are the values from the Zhang/Berry structures, including the 16.3 Å edge-to-edge value for the chicken heart complex and the closer distances in the beef and rabbit structures. The closest possible distance from the structure of Xia et al. (*1*) gives a maximal rate 5 orders of magnitude too slow. These values represent the fastest possible reaction times; more realistic estimates of the rate constant need to take account of probable reorganization energies, λ (*7*, *27*, *33*). Taking the distance from the beef hexagonal crystals between Nϵ2 of H161 of the Rieske protein, which provides one of the ligands to the [2Fe-2S] cluster, and an oxygen atom of heme propionate D (~3.4 Å), or the edge of the heme π-bonded system at the Nϵ2 atom (8.1 Å), we can calculate approximate rates of electron transfer from the [2Fe-2S] center to the heme of cyt c_1 of $\sim 3 \times 10^9$ s^{-1} and $\sim 10 \times 10^6$ s^{-1}, respectively, assuming nonadiabatic electron tunneling with a reorganization energy of 1.0 electron volts and ΔG of zero. These rates are significantly faster than measured rates for this reaction (*6*). In the native chicken crystals the distance is 14.4 Å, which would give a rate of $\sim 1.8 \times 10^3$ s^{-1} with the same assumptions, considerably slower than the rates observed in the presence of myxothiazole. If these values are realistic, they suggest that the variation in distances between crystal structures must reflect a dynamic situation, in which the ISP can reach the more intimate docking with the cyt c_1 with high probability during the <10 μs reaction time observed. In the crystals with stigmatellin (*2*), or in the tetragonal beef crystals (*1*) the shortest distance from the cluster or its ligands to the heme tetrapyrrole ring is 27 Å, giving a rate of $\sim 10^{-4}$ s^{-1} (with the same assumptions), making it very unlikely that the enzyme could function if this conformation represented a static structure.

The treatment above is appropriate for a solid-state system in which the redox centers are fixed and the reorganization energy pertains to reactant and product sharing a common protein environment. It may therefore be appropriate for reaction from a complex of lifetime long compared to the reaction rate. It seems very likely that such a long-lived reaction complex is formed between QH_2 and ISP^{ox} at the interface on cyt *b* (*4*, *35*, *36*) (see Figure 1) and that reaction to form the semiquinone proceeds from such a complex. However, the movement of the mobile head introduces a more dynamic element into the overall reaction mechanism, with properties of both first- and second-order processes. Because the movement is locally constrained, the concentration terms will be unitary, and the reaction rate will not vary with concentration of the bc_1 complex and will appear to be first-order. However, the local mechanism will include a collisional component, and the overall rate at either reaction interface will be determined by the probability of forming a reaction complex and will therefore be determined by reaction parameters, including local concentration of substrates and binding coefficients, and by diffusion. The extent to which the rates of partial reactions will be determined by these stochastic processes will depend on the stability of the reaction complexes.

Diffusional Constraints. The displacement of the ISP from the position in native crystals to the position in stigmatellin-containing crystals does not involve any significant displacement of the membrane anchor but rather an extension of the connecting loop and a rotation of 57−63°. To a first approximation, this can be modeled as a constrained diffusion, with root-mean-square displacement given by $\langle x \rangle^2 = 2Dt$ for the one-dimensional case. With a diffusion coefficient of $\sim 10^{-6}$ cm^2·s^{-1} appropriate for a small protein in an

aqueous environment, a displacement of this order (~16−22 Å) would require ~13−25 ns. This gives a minimal time for the reaction. A more complex displacement than the simple rotation about a virtual axis that seems to account for the movement, or some element of higher dimensionality in the diffusional space, would increase this time. The time for reaction will include this minimal time but be greater by a factor representing stochastic exploration of the binding domains to find configurations needed for efficient electron transfer (the on rate constants), the probabilities for dissociation from bound states (the off rate constants), and changes in on and off rate constants as the nature of the reaction complex changes on electron transfer. Some appreciation of the relative values for some of these parameters can be obtained by a consideration of the binding constants involved.

Estimates for Equilibrium Constants for Binding of the Iron Sulfur Protein at Different Sites. The order of magnitude of some of the forces involved in constraining the ISP can be derived from data in the literature. These include the binding energies associated with the change in $E_{m,7}$ of the [2Fe-2S] center induced by inhibitors, and estimates of the occupancy of the state giving rise to the $g_x = 1.800$ EPR signal of the ISP. Some of the different states of binding for the ISP in the bc_1 complex are represented in the scheme below. We assume that the lower potential redox centers of the complex (b_H, b_L) are in the oxidized state, and the Q_o site is initially vacant, conditions appropriate for both sets of crystallographic data.

$$ISP^{ox}_{C*} \overset{1/K^{\circ}_{cryst}}{\leftrightarrow} ISP^{ox}_{C} \overset{1/K^{\circ}_{c1}}{\leftrightarrow} ISP^{ox}_{free} \overset{K^{\circ}_{cytb}}{\leftrightarrow} ISP^{ox}_{B} \overset{K^{\circ}_{stg}}{\leftrightarrow} ISP^{ox}_{B-stg}$$

$$ISP^{red}_{C*} \overset{1/K^{r}_{cryst}}{\leftrightarrow} ISP^{red}_{C} \overset{1/K^{r}_{c1}}{\leftrightarrow} ISP^{red}_{free} \overset{K^{r}_{cytb}}{\leftrightarrow} ISP^{red}_{B} \overset{K^{r}_{stg}}{\leftrightarrow} ISP^{red}_{B-stg}$$

$$ISP^{red}_{B} \overset{K^{r}_{UHDBT}}{\leftrightarrow} ISP^{red}_{B-UHDBT}$$

$$ISP^{ox}_{B} \overset{K^{\circ}_{UHDBT}}{\leftrightarrow} ISP^{ox}_{B-UHDBT}$$

For binding of quinone species to the reduced ISP in the ISP_B position:

$$ISP^{red}_{B} \overset{K^{r}_{Q}}{\leftrightarrow} ISP^{red}_{B-Q}$$

$$ISP^{red}_{B} \overset{K^{r}_{QH2}}{\leftrightarrow} ISP^{red}_{B-QH2}$$

In the scheme, we indicate that the mobile head of the ISP can be free or specifically associated with reaction interfaces on cyt *b* or on cyt c_1. The superscripts o and r refer to the redox state of the [2Fe-2S] center of the protein (oxidized or reduced, respectively); the redox states can be interrelated through reaction with an arbitrary redox couple:

$$D + ISP^{ox}_{free} \leftrightarrow ISP^{red}_{free} + D^{+} \qquad K_{o/r}$$

Some uncertainty in the attribution of binding constants comes from uncertainty as to the redox status of the complexes during crystallographic analysis. The uncertainty is compounded by the possibility that reductant may be generated in the crystals by X-ray irradiation. In the discussion below, it should be recognized that any relation between equilibrium constants for reactions with partners in mixed redox states includes implicitly a $K_{o/r}$ term of unknown value.

Apart from $K_{o/r}$, all *K* terms denote association constants. The subscripts C*, C, free, B, and B-nnn (where nnn is stg, UHDBT, Q, or QH_2) designate the binding states for the ISP head as follows: C*, bound at the cyt c_1 interface, with an additional force from differential effects of crystal contacts between C and B interfaces; C, bound at the cyt c_1 interface; free, not specifically bound; B, bound at the cyt *b* interface; B-nnn, liganded by the occupant of the Q_o binding pocket (stigmatellin, UHDBT, Q, or QH_2).

The forces constraining the ISP head to a particular state are represented by equilibrium (association) constants, so that the transition from the free state to any particular bound state can be represented by the product of equilibrium constants for partial reactions, as shown in the scheme above and discussed below. The terms K_{cryst} are included to cover differences between data from different labs attributable to differences in crystals used. These could include different crystal contacts (likely the dominant term), different redox states, and different amounts of quinone in native crystals. The scheme could be expanded to include terms for the complex in different redox states of the cyt *b* and cyt c_1 hemes, but few data are available to justify the additional complexity.

Calculation of Occupancy from the Crystallographic Data. We have used ICOEFL from the CCP4 suite of programs (*22*−*24*) to estimate the occupancy of the ISP in different positions in different crystals, as summarized in Tables 1−3. This set of data makes it possible to estimate some of the binding constants from the scheme above. We recognize that the treatment used here is somewhat simplistic, but we note that the calculation of occupancy for the stigmatellin-induced position gave a value close to 1, as expected from the strong ligand between the ISP and the inhibitor. With this as a mark of confidence, we might expect that occupancies for other states would sum to 1. For the weaker binding cases, it would not be surprising to find a fraction of the ISP head in the free configuration (and therefore disordered), and we suggest that this is the simplest explanation for the missing occupancy in the native, myxothiazole, MOA-inhibitor, and UHDBT crystals. With this assumption, we can calculate association constants directly but recognize that these values should be used with appropriate caveats. One source of error might be an overestimation of occupancy from inclusion of the anchored tail in the calculation. We have eliminated this by using data from the mobile head alone (Tables 1−3). Another source of error would arise from the averaging of occupancies for the two ISP positions within a dimer, since the crystal packing is not the same for both monomers. We have looked for evidence for this by using two different methods of calculating occupancies for the two monomers independently (Tables 2 and 3), and we conclude that there is not a large difference between the monomers in our structures (but see ref *3*). We have made similar calculations after separate refinement of five contributions to the structure, with the ISP in the four separate potential locations in the two monomers treated separately. Errors in values derived from the crystallographically estimated association constants could

arise from additional liganding terms. Although both groups prepared their crystals under aerobic conditions and assumed that the redox centers were oxidized, the possibility exists of reduction by electrons arising from X-ray irradiation. The uncertain redox status of the complex in the crystals and the variability of quinone content might also contribute to the variability of the data and the differences between our structures (*2*) and that of Xia et al. (*1*). Despite these considerations, the results show an encouraging internal consistency, which suggests that the values are reasonable.

Association Constants for the Oxidized ISP. The distribution of the oxidized ISP is determined by its association constants for occupancy of interfaces on cyt *b* and cyt c_1 and by the changes in these values due to crystal contacts or other liganding interactions. The ISP subunit was disordered in the crystals of Xia et al. (*1*), which did not have crystal contacts in this region. This lack of contacts likely contributed to the disorder but perhaps also allowed the ISP to bind to the cyt *b* interface. The ISP in each of the structures of Zhang et al. (*2*) showed crystal contacts, but these contacts were slightly different in different structures and between the ISP subunits of different monomers. In the $P6_5$ crystals of Iwata et al. (*3*), the monomer with the intermediate structure showed crystal contacts. The data of Tables 2 and 3 suggest that differences between monomers in our structures were not large and that relative association constants are $K°_{cryst} < 1$, $K°_{cryst*} > 1$, $K°_{cryst*}\,K°_{c1} > K°_{cytb}$, and $K°_{cryst}K°_{c1} \leq K°_{cytb}$.

In the crystals of Xia et al. (*1*), the density of the [2Fe-2S] center measured at the Fe edge was 11.1, compared with 20.7 for heme b_H (the iron with the highest density). Since the [2Fe-2S] center has two irons, the density was 0.28 times that expected, assuming an occupancy of 1 for heme b_H. Kim et al. (*4*) report a value of 0.18 from a different data set. These values give occupancies for the ISP_B configuration, from which a range of values for the association constant (0.22−0.39) can be calculated, assuming that all the unaccounted ISP was free. For the crystals of Zhang et al. (*2*), the data of Table 1 show occupancies of 0.46−0.7 and 0.0003−0.118 for the ISP_C and ISP_B configurations, respectively. Assuming that the unaccounted density reflects unbound ISP heads (in the ISP_{free} state), we obtain the following (means from seven values for native structures treated by the different methods): $K°_{cryst*}K°_{c1} = 1.47 \pm 0.55$ and $K°_{cytb} = 0.15 \pm 0.09$, which can be compared to the value, $K°_{cytb} = 0.22-0.39$, calculated from the iron densities of Xia et al. (*1*).

We have considered above that the difference between the occupancies in the structures of Xia et al. (*1*) and our own might be explained by crystal contacts that introduce differential stability to the protein on the cyt *b* or cyt *c* side of the complex. Since the occupancy of the ISP_C position was undetected in the structure of Xia et al. (*1*) (but see ref *4*), we cannot make any estimate of the relative affinities of the two positions. Nevertheless, the occupancy of the ISP_B position in our crystals was substantially less than in the crystals of Xia et al. (*1*), so it seems likely as argued above that a major contribution to the term $K°_{cryst*}\,K°_{c1}$ must come from $K°_{cryst*}$. From this and from the relative occupancies in the crystals of Xia et al., we can assume that $K°_{c1} < 1$. The values of association constants for the oxidized ISP for both of its docking interfaces are therefore in the range of unity, given binding forces $<RT$. It therefore seems probable that the barriers to exchange between states are small and that thermal energy will be sufficient to allow the ISP to explore all states with some probability of occupancy in a time scale of the measured reaction time.

Relative Affinities of the ISP for the Interface on Cyt b in the Presence of Inhibitors. The change in E_m of the [2Fe-2S] center induced by stigmatellin or UHDBT reflects the differential binding to the reduced and oxidized forms of the ISP (*21*, *23*, *24*). Since neither binding constant is known independently, we do not know the absolute value of either. The changes in redox midpoint potential reported are $\Delta E_{m,7} \sim 220$ mV induced by stigmatellin and $\Delta E_{m,7} \sim 80$ mV induced by UHDBT. From these values, $K^r_{stg}/K°_{stg} \sim 5000$, and $K^r_{UHDBT}/K°_{UHDBT} \sim 20$. In the presence of stigmatellin in the chicken complex, all the ISP (within error) was found at the cyt *b* interface, as would be expected from the high affinity for the reduced ISP shown above. Crystals of the chicken complex containing UHDBT showed a weaker occupancy of the ISP_B position than those with stigmatellin (see Table 1), from which $K^r_{stg} > K°_{cryst*}K°_{c1}/K°_{cytb}$ and $K^r_{UHDBT} \approx K°_{cryst*}K°_{c1}/K°_{cytb}$. From the values in Table 1 and using the same assumptions as for the native crystals, we can calculate association constants for ISP^{red} in the UHDBT crystals for comparison with those in the native crystals, $K°_{cryst*}K°_{c1} = 1.46 \pm 0.76$. This is in good agreement with the value from the native complex, suggesting that UHDBT does not affect the affinity for the cyt c_1 interface. The affinity for the cyt *b* interface was markedly increased, to give $K^r_{UHDBT}K°_{cytb} = 0.99 \pm 0.38$. By use of the average value for $K°_{cytb}$ given above, $K^r_{UHDBT} \approx 6.53$, which can be compared with the relative affinities of the inhibitor for reduced and oxidized forms of the ISP given above (a value of ∼20).

The values for binding constants in the presence of stigmatellin and UHDBT are appropriate only if the binding species was the reduced form. Addition of stigmatellin or UHDBT at ambient potential to the bc_1 complex in situ or in detergent suspension induces a reduction of the ISP, presumably from endogenous reductant, in response to the removal of the reduced form from the redox equilibrium of the free form. We might suppose that this reduction by adventitious donor also occurred in the cocrystals with stigmatellin or UHDBT.

Values for association constants similar to those for the native complex were obtained from the data in the presence of myxothiazole or the MOA-type inhibitors (Tables 1 and 3). A trend in the occupancy values for the ISP_B position toward a loss of occupancy from the cyt *b* interface was apparent, suggesting that either occupancy of the proximal domain or displacement of quinone by these inhibitors might weaken the affinity of the cyt *b* interface for ISP^{ox}. Kim et al. (*4*) observed a more dramatic loss of the anomalous Fe density from the cyt *b* docking configuration in crystals with MOA-stilbene. The structural difference associated with myxothiazole binding, showing a closing of the access between the Q_o pocket and the aqueous phase at the ISP-binding interface (*35*), might contribute to this differential binding of the ISP^{ox}. Other data from the recent analysis by Kim et al. (*4*) of occupancy of the [2Fe-2S] cluster in structures with and without inhibitors, using the anomalous difference data, show a similar pattern of effects

of inhibitors to that reported here.

Relative Binding Constants for Oxidized and Reduced ISP at the Cyt b Interface. The change in EPR spectrum of the ISP to give a band at $g_x = 1.80$ is ascribed to the ligation of the reduced ISP by quinone bound in the distal domain of the Q_o site (*25*). De Vries et al. (*41*) analyzed the spectrum of the ISP under conditions in which the $g_x = 1.80$ signal was formed and could fit the spectrum with two components. Component 1 included a sharp peak at $g_x = 1.8046$, which broadened on reduction, to give a shape more similar to that of component 2. De Vries et al. (*41*) interpreted the two spectral components seen when the pool was oxidized as two separate species. If we interpret the two components as two forms of the same species, corresponding to ISP^{red} liganded with Q (component 1) and unbound ISP^{red} (component 2), the results suggest that less than half the ISP^{red} was in the ISP_B configuration, to give $K_A \sim 0.8-1$. The relatively small amplitude of the overshoot in the experiments of Figures 2 and 4 could indicate a value as low as 0.2. Preliminary results from fluorescence quenching experiments using labeling of specifically engineered cysteine residues on ISP and cyt *b* with complementary fluorophores (*42*) suggest a value for $K_A \sim 2.3$, giving $K^r_Q K^r_{cytb} \approx 0.2-2.3$.

Since the E_m value at which the $g_x = 1.80$ signal appears on redox titration is close to that of the quinone pool, the binding constants of the site under these conditions (ISP^{red}) for Q and QH_2 must be similar, suggesting that $K^r_Q \approx K^r_{QH2}$. However, it is unlikely that the ISP^{red} binds with the same affinity when QH_2 rather than Q occupies the pocket. Fluorescence quenching data from FRET experiments (*42*) show that the ISP^{red} moves away from cyt *b* on reduction of the quinone pool, suggesting that ISP^{red} does not form a ligand with QH_2 at the Q_o site. A more complete description requires partitioning of the binding equilibria into partial contributions and introduction of additional terms:

$$Q + \text{vacant}\cdot b + ISP^{red}_{free} \overset{K_Q^{ass}}{\leftrightarrow} Q_o\cdot b + ISP^{red}_{free} \overset{K_{ISP}^{lig}}{\leftrightarrow} Q_o\cdot b\cdot ISP^{red}_{B} \quad (3)$$

If the ligand between QH_2 and ISP^{red} is absent or much weaker than that with Q, then the apparent equal affinity of the site for Q and QH_2 would indicate that the protein provides an additional binding free energy for the QH_2 to compensate for the differential ligation by ISP^{red}:

$$QH_2 + \text{vacant}\cdot b + ISP^{red}_{free} \overset{K_{QH2}^{assn}}{\leftrightarrow} Q_oH_2\cdot b + ISP^{red}_{free} \overset{K_{ISP}^{c}}{\leftrightarrow} Q_oH_2\cdot b \text{ - - - } ISP^{red}_{C} \quad (4)$$

$$K_Q^{overall} = K_Q^{assn} K_{ISP}^{lig} = K^r_Q K^r_{cytb} = 0.8-2.3$$

$$K_{QH2}^{overall} = K_{QH2}^{assn} K_{ISP}^{c}$$

The apparent E_m value observed in titrations of the occupancy of the Q_o site when the ISP is reduced will include the right-hand terms in eqs 3 and 4. Since $K_Q^{overall} \approx K_{QH2}^{overall}$:

$$E_m(Q/QH_2, \text{pool}) \approx E_m(Q_o\cdot b\cdot ISP^{red}_{B}/Q_oH_2\cdot b \text{ - - - } ISP^{red}_{C})$$

If $K_Q^{overall}$ includes a liganding force, K_{ISP}^{lig}, then K_{QH2}^{assn} must be greater than K_Q^{assn} by a value equal to $K_{ISP}^{lig}/K_{ISP}^{C}$. It seems possible that this might account for some of the higher apparent association constant for QH_2 seen in kinetic experiments. As noted in the companion paper (*25*), from recently refined structures of the complex with stigmatellin (2bcc and revised 3bcc), Glu-272 provides a ligand to the OH group of the inhibitor, with the latter acting as H-bond donor. We have suggested that this side chain might also provide a ligand to quinol, with the OH of quinol as H-bond donor. In the native crystals, the side chain is rotated out of the site. We suggest that this is the configuration when quinone occupies the site, since the carbonyl group will not provide a H-bond donor. The differential binding ($K_{QH2}^{assn}/K_Q^{assn}$) likely reflects this H-bond. Mutant strains with Glu-272 changed to D or G (E295D or -G in *Rb. sphaeroides* numbering) showed apparent K_m values for quinol substrate greater by 1.54- and 2.4-fold respectively, suggesting that this was a relatively weak contribution.

As suggested by Crofts and Wang (*6*) and discussed in a companion paper (*25*), the activated step in electron transfer, and the rate-limiting step at saturating substrate concentration, is the oxidation of bound quinol. We have suggested that the reaction proceeds from an ES complex formed between ISP^{ox}, docked in the ISP_B position, and quinol in the distal domain of the Q_o site (*12*, *25*). To account for the maximal rates of quinol oxidation observed when the pool is substantially oxidized, Crofts and Wang (*6*) modeled the reaction with a differential binding of QH_2 and Q of 30−50-fold. It seems likely that the structure with stigmatellin demonstrates the location of all complexes formed between the Q_o site occupant and the ISP, including the reaction complex (*12*, *21*, *25*, *43*). The bond between the carbonyl group of the inhibitor and His-161 of the ISP might mimic that between quinone and ISP^{red}. However, the ES complex would involve a bond between the OH of the quinol and His-161 of the ISP^{ox} (*25*, *42*, *44*). Since the H-bond provided by Glu-272 likely provides only a factor of ~2.5 of the 30−50-fold differential binding of quinol (see above), we suggest that the major part, a factor of 10−20, is contributed by the liganding of quinol by the ISP^{ox} through His-161.

CONCLUSIONS

We have demonstrated that all the reactions of the high-potential chain through which oxidizing equivalents are delivered to the quinol oxidizing site are rapid compared to the rate-limiting step of quinol oxidation. For those reactions accessible to direct measurement, the activation energies were much lower than that of the overall process. For those reactions for whose rate constant we can only estimate a lower limit, it is clear that there is no contribution to the rate-limiting step and neither therefore to the activation barrier. The movement of the ISP between catalytic interfaces must therefore occur much more rapidly than the rate-limiting steps for the partial reactions measured. From the lack of transient overshoot in the high-potential chain inhibited by myxothiazole, the electron donation from the [2Fe-2S] in the ISP_C position is < 10 μs. From the 150 μs lag before cyt *b* reduction and the rise times of the constituent processes, the transfer of an oxidizing equivalent from ferricyt c_1 to the Q_o site occurs in <50 μs. We have shown that diffusion

of the mobile head of the ISP is expected to be rapid, with a time for root-mean-square displacement over the ~16−22 Å diffusion distance in the range <25 ns. We have estimated the binding constants for the interactions of the ISP with its two interfaces and shown that with the exception of specific ligands between occupant and the ISP, the association constants are <2. Absolute values for on and off rate constants are not available, but we anticipate that the on rate constants will be determined by the collisional frequencies and an additional time for stochastic exploration of the docking interfaces. Since these will reflect the rapid diffusion constrained to a local domain by the tethering of the head, we can expect an efficient exploration of the docking domains to find a suitable reaction configuration. Since the apparent association constants calculated from the crystallographic occupancies are all within the range <2, the off rate constants must have values similar to the on rate constants. The range of calculated values for the processes associated with the movement of the ISP are therefore in accord with the limits on rate determined from kinetic measurements. Both on and off rate constants are certainly greater than the values $>2 \times 10^4$ s^{-1} indicated by our measurements of the overall processes.

The kinetic picture that emerges from these considerations is of a rapid process, in which electrons are transferred efficiently over a distance, without the entropic loss of diffusion in the volume of the aqueous phase. By tethering the head, the complex maintains a high local concentration and a high probability of successful collision. Although the rates achieved are comparable to those expected from a solid-state system with an intermediate electron carrier, we do not believe that the evolution of this mechanism was determined by the need for rapid electron transfer. Rather, the mechanism fits the site for the peculiar needs of the bifurcated reaction, which we discuss at length in a companion paper (*25*). We see no evidence that protein−protein interactions lead to specific binding to constrain the ISP^{ox} in particular positions and suggest that catalytic switching is determined more by the liganding with the Q_o site occupant in the ES complex than by other protein interactions. However, we have noted that significant conformational changes accompany binding of inhibitors, and these may mimic changes on occupancy of the different domains of the Q_o site by reaction intermediates (*12*, *13*, *25*). It seems possible that such changes might hinder movement of the ISP through physical blockage and that linkage to Q_o site domain occupancy might provide a switching function.

REFERENCES

1. Xia, D., Yu, C.-A., Kim, H., Xia, J.-Z., Kachurin, A. M., Zhang, L., Yu, L., and Deisenhofer, J. (1997) *Science 277*, 60−66.
2. Zhang, Z., Huang, L., Shulmeister, V. M., Chi, Y.-I., Kim, K. K., Hung, L.-W., Crofts, A. R., Berry, E. A., and Kim, S.-H. (1998) *Nature (London) 392*, 677−684.
3. Iwata, S., Lee, J. W., Okada, K., Lee, J. K., Iwata, M., Rasmussen, B., Link, T. A., Ramaswamy, S., and Jap, B. K. (1998) *Science 281*, 64−71.
4. Kim, H., Xia, D., Yu, C. A., Xia, J. Z., Kachurin, A. M., Zhang, L., Yu, L., and Deisenhofer, J. (1998) *Proc. Natl. Acad. Sci. U.S.A. 95*, 8026−8033.
5. Crofts, A. R., and Berry, E. A. (1998) *Curr. Opin. Struct. Biol. 8*, 501−509.
6. Crofts, A. R., and Wang, Z. (1989) *Photosynth. Res. 22*, 69−87
7. Meinhardt, S. W., and Crofts, A. R. (1982). *FEBS Lett. 149*, 223−227.
8. Tsai, A.-L., Olson, J. S., and Palmer, G. (1983) *J. Biol. Chem. 258*, 2122−2125.
9. Moser, C. C., Page, C. C., Farid, R., and Dutton, P. L. (1995) *J. Bioenerg. Biomembr. 27*, 263−274.
10. Gray, H. B., and Winkler, J. R. (1996) *Annu. Rev. Biochem. 65*, 537−561.
11. Bowyer, J. R., Dutton, P. L., Prince, R. C., and Crofts, A. R. (1980) *Biochim. Biophys. Acta 592*, 445−460.
12. Crofts, A. R., Barquera, B., Gennis, R. B., Kuras, R., Guergova-Kuras, M., and Berry, E. A. (1999) in *The Phototrophic Prokaryotes* (Peschek, G. A., Loeffelhardt, W., and Schmetterer, G., Eds.) pp 229−239, Plenum, New York.
13. Crofts, A. R., Guergova-Kuras, M., Huang, L.-S., Kuras, R., Zhang, Z., and Berry, E. A. (1999) Mechanism of ubiquinol oxidation by the bc_1 complex: role of the iron sulfur protein and its mobility, *Biochemistry 38*, 15791−15806.
14. Woese, C. R. (1987) *Microbiol. Rev. 51*, 221−271.
15. Degli Esposti, M., De Vries, S., Crimi, M., Ghelli, A., Patarnello, T., and Meyer, A. (1993) *Biochim. Biophys. Acta 1143*, 243−271.
16. Gennis, R. B., Barquera, B., Hacker, B., van Doren, S. R., Arnaud, S., Crofts, A. R., Davidson, E., Gray, K. A., and Daldal, F. (1993) *J. Bioenerg. Biomembr. 25*, 195−210.
17. Mitchell, P. (1976) *J. Theor. Biol. 62*, 327−367.
18. Crofts, A. R., Meinhardt, S. W., Jones, K. R., and Snozzi, M. (1983) *Biochim. Biophys. Acta 723*, 202−218.
19. Crofts, A. R. (1985) in *The Enzymes of Biological Membranes* (Martonosi, A. N., Ed.) Vol. 4, pp 347−382, Plenum, New York.
20. Brandt, U., and Trumpower, B. L. (1994) *CRC Crit. Rev. Biochem. 29*, 165−197.
21. Link, T. A. (1997) *FEBS Lett. 412*, 257−264.
22. Jones, T. A. (1992) *Proceedings of the CCP4 Study Weekend, Molecular Replacement* (Dodson, E. J., Glover, S., and Wolf, W., Eds.) pp 91−105, The SERC (U.K.) Collaborative Computing Project No. 4, Daresbury Laboratory, Warrington, U.K.
23. CCP4 (1995) The CCP4 Suite: Programs for Protein Crystallography. *Acta Crystallogr. D50*, 760−763.
24. Jones, T. A., Zou, J. Y., Cowan, S. W., and Kjeldgaard, M. (1991) *Acta Crystallogr. A47*, 110−119.
25. Crofts, A. R., Barquera, B., Gennis, R. B., Kuras, R., Guergova-Kuras, M., and Berry, E. A. (1999) Mechanism of ubiquinol oxidation by the bc_1 complex: different domains of the quinol binding pocket and their role in mechanism and binding of inhibitors, *Biochemistry 38*, 15807−15826.
26. Matsuura, K., Bowyer, J. R., Ohnishi, T., and Dutton, P. L. (1983) *J. Biol. Chem. 258*, 1571−1579.
27. Link, T. A., Haase, U., Brandt, U., and von Jagow, G. (1993) *J. Bioenerg. Biomemb. 25*, 221−232.
28. Schägger, H., Brandt, U., Gencic, S., and von Jagow, G. (1995) *Methods Enzymol. 260*, 82−96.
29. Meinhardt, S. W., and Crofts, A. R. (1982) *FEBS Lett. 149*, 217−222.
30. Ding, H., Robertson, D. E., Daldal, F., and Dutton, P. L. (1992) *Biochemistry 31*, 3144−3158.
31. Ding, H., Moser, C. C., Robertson, D. E., Tokito, M. K., Daldal, F., and Dutton, P. L. (1995) *Biochemistry 34*, 15979−15996.
32. Ding, H., Daldal, F., and Dutton, P. L. (1995) *Biochemistry 34*, 15997−16003.
33. Bowyer, J. R., and Crofts, A. R. (1978) in *Frontiers of Biological Energetics* (Dutton, P. L., Leigh, J., and Scarpa, A., Eds.) Vol. I, pp 326−333, Academic Press, New York.
34. Meinhardt, S. W., and Crofts, A. R. (1983) *Biochim. Biophys. Acta 723*, 219−230.
35. Glaser, E. G., and Crofts, A. R. (1984) *Biochim. Biophys. Acta 766*, 322−333.
36. Tian, H., Yu, L., Mather, M. W., and Yu, C.-A. (1998) *J. Biol. Chem. 273*, 27953−27959.

37. Gatti, D. L., Meinhardt, S. W., Ohnishi, T., and Tzagoloff, A. (1989) *J. Mol. Biol. 205*, 421−435.
38. Van Doren, S. R., Gennis, R. B., Barquera, B., and Crofts, A. R. (1993) *Biochemistry 32*, 8083−8091.
39. Denke, E., Merbitzzahradnik, T., Hatzfeld, O. M., Snyder, C. H., Link, T. A., and Trumpower, B. L. (1998) *J. Biol. Chem. 273*, 9085−9093.
40. DeVault, D. (1980) *Q. Rev. Biophys. 13*, 387−564.
41. De Vries, S., Albracht, S. P. J., and Leeuwerik, F. J. (1979) *Biochim. Biophys. Acta 546*, 316−333.
42. Crofts, A. R., Berry, E. A., Kuras, R., Guergova-Kuras, M., Hong, S., and Ugulava, N. (1998) in *Photosynthesis: Mechanisms and Effects* (Garab, G., et al., Eds.) Vol. III, p 1481−1486, Kluwer Academic Publishers, Dordrecht, the Netherlands.
43. Lancaster, C. R., and Michel, H. (1995) in *Reaction centers of photosynthetic bacteria. Structure and Dynamics* (Michel-Beyerle, M. E., Ed.) International Workshop Feldafing III, Springer-Verlag, Berlin.
44. Ugulava, N., and Crofts, A. R. (1998) *FEBS Lett. 440*, 409−413.

BI990963E